2010 IEEE International Conference on Robotics and Automation
Anchorage Convention District
May 3-8, 2010, Anchorage, Alaska, USA

Intuitive Human Skill Reconstruction for Compliance Control

Samuel Okodi, Xin Jiang, Satoko Abiko, Atsushi Konno and Masaru Uchiyama
Graduate School of Engineering, Tohoku University
Aoba-yama 6-6-01, 980-8579 Sendai City, Japan Fax: +81-22-795-6971,
e-mail: okodi, jiang, abiko, konno, uchiyama@space.mech.tohoku.ac.jp

Abstract— **This paper presents a robust and efficient method of generating manipulation motion skill for non-force-feedback high speed constrained compliant robot motion. Using a non-structured teaching environment, the inherent task in the captured demonstration force and position data is estimated and reconstructed from three sets of complimentary models, including analytical mathematical modelling, empirical modelling and human skill demonstration modelling. The approach addresses task specification accuracy deficiencies, and involves outward interface simplifications, with embedded rigorous analytical methodologies that enable users to realise complex and robust constrained compliant robot motion without dealing with the low level motion generation aspects. Function based task representation supports an intuitive approach to generate robust constrained motion by skill superimposition, as exemplified by peg-in-hole with crank turning.**

I. Introduction

A general efficient method of generating non-force-feedback compliant robot manipulation motion skill for control is addressed in this paper. Prior motion creation for high speed, accurate 6-DOF motion with dexterous intuitive skill required long setup times, with discrete and heuristic human inputs. That is a strenuous and unproductive process [1]. Demonstrative teaching [2], [3] replaced discrete parameter specification [1] to provide a fast trajectory [3] and a fast initial task shape [2], albeit with little flexibility. Implementing fast, efficient, flexible and robust task reconstruction eluded the teaching methods. Generating consistent robot motion in [1]–[3] required an inflexible similar structured external teaching task-specific workspace; the teaching required human involvement to provide the teach-to-robot workspace transformations; [2] was not general and required human input at one stage.

Task data representation from human demonstrations as a regular function leads to: using statistical approaches to estimate the data trend as an *a priori* regular function, application of mathematical operations to the regular functions to achieve complex tasks, estimation methods to recover from irregular demonstration and non-structured workspaces, and flexible virtual environments. This work lays a foundation for simultaneous force, position and stiffness from the same external task demonstration.

In the preceding work [2], task representation was amorphous. In this work, representation is solved by estimation and regular function fitting. Estimation of highly irregular demonstration trajectories lays a foundation on which position, force and stiffness are simultaneously estimated efficiently from the same demonstration setup.

Much work on robot force control applies hybrid force-position control [4], compliant robot motion, applying adaptive control, and analysis of contact formation [5], [6]. Blind searching strategies [7] and geometric analysis strategies implement feedback force control. Faster motion capability is achieved in this work by enhancing the task without force feedback [1]. Direct drive (DD) actuated parallel robots achieve constrained compliance control using the task frame formalism with no environment force sensing, set stiffness of each DOF is selected for the robot. Motion from human demonstration using "atomic" motion macros has been presented [8]–[10], such macros ease motion generation, but inefficiently represent dexterity from expert demonstrations.

A multiple-model task reconstruction (MMTR) approach is used, it is a fast and reliable method to augment human motion, dexterity and skill techniques acquired from task demonstration, use intuition, apply analytic mathematical estimation to represent the tasks, and determine heuristic model based parameters. The independent models collectively used are sufficient to completely reconstruct a robust constrained motion task. By feed-forward reference position, force and stiffness of the end effector, robust and high speed constrained robot motion is achieved without force feedback. To regulate the contact force, a combination of motion technique, stiffness, accuracy and force are used. An algorithm implements an artificial mind on the multiple models to reconstruct the inherent assembly task from the demonstration data. Augmented with intuitive human skill, synthesis of complex robot skills is semi-autonomously achieved, saving time from dealing with the data level underlying aspects of the process. The peg-in-hole with crank turning task is used for validation.

In the paper, Section II presents the robot system and the heuristic empirical model emulated and generalised by the algorithm, which is also used to evaluate the compliance and trajectory following result. Section III presents the task models used to reconstruct human demonstration skills, experimental parameters, skill reconstruction and the intuition integration algorithm. Section IV discusses the results of reconstructing human demonstration data with algorithmic logic to emulate the empirical heuristic skill, and improvements by analytical methods to further estimate and replace amorphous position data with regular function, augmenting a regular function with intuitive skill and the effect on constrained motion performance. A conclusion and future work concludes the paper in Section V.

II. Setup and Experiments

A. Human Motion Capture System

Raw human task position data for a structured environment demonstration is captured at 50 [Hz] by a Xeon 3.2GHz Nexus™server and 8 Vicon™MX cameras for markers placed around a force-torque sensor, force is captured at 115200 [baud] by BL Autotec 10kg-f/100kg-f-cm force-torque sensors (FTS), running on an embedded Pentium III 750 MHz CPU running a VxWorks 6.2 ™system, the VxWorks remote controls the Nexus motion capture system for start and end synchronisation.

B. Virtual Motion Generation

The virtual motion generation and kinematics simulator runs on a CentOS 4.5 Linux Pentium IV 3.2GHz CPU with a C++ integrated glade GUI for parameters specification; an SGI-OpenInventor 3D for virtual simulation; and MatLab 2006a.

C. Experiment Robot

The experiment robot is a Pentium IV 2.4GHz VxWorks 6.1 real time control embedded computer for a HEXA parallel robot. HEXA is a 6-degree-of-freedom high speed position, force and compliance mode controlled parallel robot, capable of constrained motion control without force feedback in the control law [1], [2].

III. The Multiple Task Models

To robustly enhance constrained compliance motion required heuristic human input, making the method strenuous and unproductive. In this work, instead of discrete specifying or computing the entire robot trajectory, teaching is used, which reduces trajectory generation complexity by providing a starting general task shape, upon which analytical methods are applied to enhance the shape, profile and flexibility of the resultant task.

Among the difficulties to overcome without force feedback control is initial mating, where a substantial amount of time is required to set the control of the end effector when initiating tight-tolerance constrained motion. An operator specifies the motion primitives of the task, the amount of compliance necessary for a particular task is not known and is determined through heuristic actual robot trials, such a solution is initially time consuming, and since flexibility is the basis of such robots, long setup times hamper automated productivity.

An example of a complex human manipulation task is used to evaluate human skill reconstruction from multiple task models. Using multiple task models provides an approach of modelling the task, with each model optimised for estimation of certain particular model parameters, parameters that can not all be estimated from a single task model.

Instant robot position and force data is obtained from motion capture setups. The demonstrated raw data trajectory can not be replayed by the robot, because: 1, the data from disparate sensors in unsynchronised; 2, the precision of the position measuring equipment is less than the robot precision; 3, there is no distinction between constrained and unconstrained trajectory segments; 4, the task is amorphously defined by position data; 5, the position data is an ensemble of marker positions on objects; 6, the demonstration task does not necessarily represent the same meticulous structure of the targeted robot task. These factors necessitate: 1, a reconstruction of the task to synchronise that data; 2, to resolve accuracy deficiencies; 3, segment the motion into sections of constrained and unconstrained motion; 4, resolve ambiguities in task representation and define the task is terms of functions subject to estimation and mathematical analysis to facilitate concise representation and estimation analysis; 5, resolve the position of the object from its marker positions; 6, define *a priori* functions that estimate the task geometry of best fit on the demonstration data and define or estimate parameters necessary to ignore the meticulous demonstration space to the robot workspace structural fidelity.

A. Mathematical Methods for the Models

The mathematical models applied include the forward and inverse kinematics models [11], the least squares data geometry estimation methods, and the virtual inverse kinematics motion generation interface model [1] These models will be described where they apply.

B. The Virtual Kinematics Model (VKM)

This is an offline teaching system for generating trajectory paths in a 3D kinematics simulator. Depending on the size of force on the end effector during playback, stiffness values are assigned, so as, to accommodate deviations and deflections to minimise the anticipated contact forces. Careful construction of a task is conducted [1], [2] and optimal empirical stiffness values that minimise the reaction forces during constrained motion are heuristically determined.

C. Heuristic Parameters Model (HPM)

These are empirically determined parameters during constrained VKM-motion experiments. The parameters determine the conditions under which typical constrained robot tasks are executed by the robot. Heuristic experiments for the practical handling of the control mode transitions, and the representation of tasks in the robot workspace were established. This empirical work laid the foundation of generating similar data autonomously from task demonstrations. Ideally, by analysing the force and position data, constrained and unconstrained trajectories could be established. In the unconstrained trajectories the problem involved determining optimum trajectory paths to ensure kinematic consistence and minimise adverse contact phase instability through projecting the momentum of the end effector along the insertion axis. And determining the control mode switching distance in the vicinity of contact.

D. The Direct Teaching Model (DTM)

This is a direct (forward) kinematics application to determine locations of objects in the HEXA robot workspace. This recursive approach is built from the Newton-Raphson formulation. A Cartesian position $\boldsymbol{p} = [\ \boldsymbol{x}\ \boldsymbol{\psi}\ ]^T \in R^6$ is determined from its joint-space angular position $\boldsymbol{\theta} = [\ \theta_1\ \theta_2\ ...\ \theta_6\ ]$ by (1).

$$\boldsymbol{p}_k = \boldsymbol{p}_{m+1} : \lim_{(\boldsymbol{p}_{m+1} - \boldsymbol{p}_m) \to \epsilon} \boldsymbol{p}_{m+1} = \boldsymbol{p}_m + \boldsymbol{J}\ (\boldsymbol{\theta}_k - \boldsymbol{\theta}_m) \quad (1)$$

$$\text{where } \boldsymbol{\theta}_m = \boldsymbol{f}^{-1}(\boldsymbol{p}_m) \quad (2)$$

The iteration Equation (1), (2) converges within index $m \leq 200$. Several position data $\boldsymbol{\theta}_k : k = 1, 2, 3, ..., n$ where index k, taken when the end effector is constrained, is used to estimate the geometry of the constraint in the workspace by least squares approximation to simple geometric functions that define the contact surfaces during compliance control. $\boldsymbol{J}$ is the joint space to task space Jacobian matrix, (2) is the inverse kinematics function. An object (Fig. 1(a)), is defined by its initial position $\boldsymbol{p}_o$ and its orientation is recovered from the principal component analysis (PCA) of the points k. For a matrix $\boldsymbol{X} = [\boldsymbol{x}_1 ... \boldsymbol{x}_n]^T$, of Cartesian position data, $\boldsymbol{x}_i = [x_i y_i z_i]^T$ their data covariance matrix, $\boldsymbol{A}$, is given by $\boldsymbol{A} = \left[[(x_1 - \overline{x}) \cdots (x_n - \overline{x})]^T \quad [(y_1 - \overline{y}) \cdots (y_n - \overline{y})]^T\ [(z_1 - \overline{z}) \cdots (z_n - \overline{z})]^T\right]$

$$\text{and } \boldsymbol{U}\ \boldsymbol{S}\ \boldsymbol{V}^T = \boldsymbol{A} \quad (3)$$

$\boldsymbol{V}$, is the orientation matrix of the data principal components, $\boldsymbol{C}$ is an eigenvector corresponding to a singular value, the largest singular value in this case σ_{max}

$$\text{where } \boldsymbol{C}(\sigma_{\max}) = [\ a\ b\ c\ ]^T = \boldsymbol{V}(\sigma_{\max}) \quad (4)$$

$$\boldsymbol{x}_{tf} = \boldsymbol{x}_o + \mu \boldsymbol{C}(\sigma_{\max}) \quad (5)$$

For $\boldsymbol{A}$, $\boldsymbol{V}$ is a matrix of the orthonormal basis vectors that define the distribution of the data $\boldsymbol{X}$ about the data mean $\overline{\boldsymbol{x}}$. The line vector fit with the least total square error to the data is the eigenvector corresponding to the maximum singular value, the converse is true for the least singular value. Constrained motion is equivalent to end effector alignment with the line function (5), moving toward $\boldsymbol{p}_o$. Determining this workspace geometry calibrates the workspace with respect to the robot base reference frame Σ_b, and provides

an accurate basis to transform data from an external demonstration workspace into the robot workspace. The variable scalar μ makes trajectory positions $\boldsymbol{x}_{tf}$ from position and direction vectors $\boldsymbol{x}_o$ and $\boldsymbol{C}(\sigma_{\max})$ respectively for the task frames $\boldsymbol{p}_{tf}$.

E. The Human Demonstration Data Model (HDM)

The human demonstration data model involves analysing the demonstrated data in order to reproduce a task similar to the real or virtual teaching model, where human decision making is replaced with algorithmic logic derived from analysing the force and position task demonstration data. To synchronise the force and position data from disparate sensors, the denser force data (1.0 [KHz]) is sampled at the corresponding position frequency 50 [Hz].

1) $\boldsymbol{p}$ and $\boldsymbol{F}$ synchronisation: The raw force and pose data, $\boldsymbol{F}_i = [F_x\ F_y\ F_z\ \tau_z\ \tau_y\ \tau_x]\ i = 1, 2, ..., n$, and $\boldsymbol{p}_i = [p_x\ p_y\ p_z\ \alpha\ \beta\ \gamma]\ i = 1, 2, ..., m$, is synchronised into N_i. i specifies a discrete data point for the n^{th} data interval, $i = n\Delta t$, such that, $\boldsymbol{p}_i = p(n\Delta t)$.

$$\begin{aligned} \boldsymbol{N}_i = \boldsymbol{N}(\ \boldsymbol{p}_i, \boldsymbol{F}_i) = [\ \ \boldsymbol{p}_i, \boldsymbol{F}_i\ ] \\ i = 1, 2, 3, .., k\text{:}\ \ k = \min\{m, n\} \end{aligned} \tag{6}$$

2) Trajectory segmentation: Constrained and unconstrained segments are deduced from the measured forces, for unconstrained segment the force measured is less than a set threshold.

$$\boldsymbol{N}_{c1,c2} : \begin{cases} c1 = \min(i)\ \forall\ \boldsymbol{F}_i \geq F_{min} \\ c2 = \max(i)\ \forall\ \boldsymbol{F}_i \geq F_{min} \end{cases} \tag{7}$$

3) Insertion task-frame: Three spaces Σ_t, Σ_d and Σ_{wt} define: a demonstration task aligned reference; the base; and the robot worktable reference frames. For peg-in-hole insertion, a rigid hole is used to determine the static position bounds, these bounds are applied to the general case when the hole is not static, as is the case for crank turning. For a depth of insertion D into a hole of depth H, the orientation of the hole and $D : D_{CH} < D < H$ is recovered by applying (3)-(5). For a rigid tight insertion, the peg is fairly aligned to the hole axis after several millimetres of insertion, otherwise D should be sufficiently large to ensure that the peg is constrained inside. The data w.r.t the hole task frame ${}^t\boldsymbol{x}_i$ is:

$${}^t\boldsymbol{x}_i = \boldsymbol{V}\boldsymbol{x}_i \tag{8}$$

$${}^t\boldsymbol{x}_i - \overline{\boldsymbol{x}} = \boldsymbol{\sigma}_{vi} \tag{9}$$

the mean value of $\boldsymbol{\sigma}_{vi}$ for $\boldsymbol{p}_i$ inserted to a depth D:

$$\boldsymbol{\sigma}_v = \overline{\boldsymbol{\sigma}}_{vi}\ \ : D_{CH} < {}^t x_{3i} < D \tag{10}$$

When the hole is not rigidly fixed, as it is for inserting into a crank, the same analysis applies, but the lateral error $\Delta\boldsymbol{x}_i$ does exceed $\boldsymbol{\sigma}_v$. Three cases are identified for checking what case obtains, namely: constrained vertical, constrained lateral or unconstrained free motions. For consecutive segments of position data between $i = k_e, k_e + 1, ..., k_e + l$

$$\overline{x}_j = \frac{1}{l+1} \sum_{i=k_e}^{i=k_e+l} x_{ji} \quad j : 1, 2, 3 \tag{11}$$

$$\Sigma\Delta x_j = \sum_{i=k_e}^{i=k_e+l} |x_{ji}^2 - \overline{x}_j^2| \tag{12}$$

where l is an integer, scalar thresholds W set depending on $\boldsymbol{\sigma}_v$ are used to detect significant deviation from the current task frame of $\overline{x}$ and $\boldsymbol{V}$, and compute a new task frame.

$$\left(\Sigma\Delta^t x_1 \geq W \quad \text{or} \quad \Sigma\Delta^t x_2 \geq W\right) \text{ and } \Sigma\Delta^t x_3 \leq W_z \tag{13}$$

$$\left(\Sigma\Delta^t x_1 < W \quad \text{or} \quad \Sigma\Delta^t x_2 < W\right) \text{ and } \Sigma\Delta^t x_3 > W_z \tag{14}$$

Constrained lateral motion (13), and constrained vertical motion (14) is analysed segment by segment for a set interval of position data. Insertion into a rigid hole produces point $\boldsymbol{p}_{c3}$ which corresponds to the minimum point of insertion, and a tight value of σ_v, however if the hole is replaced by a crank, $\boldsymbol{p}_{c3}$ may occur anywhere around the cranking circle, and the maximum depth of insertion D is determined from $D + D_{CH} \approx p_{zc1} - \min(p_{zi})$.

4) Constrained lateral motion: Using the crank turning example, (13) is satisfied for the start of cranking $i = cs$ to the end of cranking $i = ce$. Over the interval $i = cs : ce$ the radius, r of the crank circle, the centre $\boldsymbol{x}_o$ and the circle orientation matrix $\boldsymbol{R}_c = \boldsymbol{V}$, are estimated [12]. The normal to the crank plane $\hat{\boldsymbol{n}}$ is the vector corresponding to minimum singular value from the PCA of the covariance matrix $\boldsymbol{A}$ for $\boldsymbol{X} = [\boldsymbol{x}_{cs}...\boldsymbol{x}_{ce}]^T$

$$\hat{\boldsymbol{n}} = \boldsymbol{V}(\sigma_{min}) \tag{15}$$

Robot skill is a combination of position, force and stiffness, therefore to maintain the velocity profile, the demonstration data down-sampling preserves the velocity profile in the subsequent task reconstruction. $n = O + 1$ the number of points between $\boldsymbol{p}_{j+1}$ and $\boldsymbol{p}_j$ must be sufficient for the maximum order of interpolation O necessary to preserve $\boldsymbol{p}$, $\dot{\boldsymbol{p}}$, and $\ddot{\boldsymbol{p}}$.

5) Task geometry reconstruction: Demonstration positions are not precisely accurate, for example: the jerky chamfer crossing position data is ill-suited for re-use. During insertion for cranking the peg may significantly move from its initial position, and the free space trajectories may not be kinematically consistent. Thus: the chamfer crossing section together with the insertion motion are reconstructed using the plane estimated normal. From the direct teaching model, the orientation of the table and the centre of the crank were determined as ${}^d\boldsymbol{R}$ and ${}^d\boldsymbol{p}_c$ respectively.

$${}^t\boldsymbol{x}_i = {}^d\boldsymbol{R}^T x_i \tag{16}$$

$${}^{wt}\boldsymbol{x}_i = {}^{wt}\boldsymbol{R}^T\ {}^t\boldsymbol{x}_i + {}^d\boldsymbol{x}_c \tag{17}$$

The orientation of the end effector is computed from the vector between $\boldsymbol{x}_c$, $\boldsymbol{x}_o$ and the normal to the plane $\hat{\boldsymbol{n}}$, and is denoted as θ_o. The subsequent points along the curve make a vector $\hat{\boldsymbol{u}}_i$. The angle about the circle normal between $\hat{\boldsymbol{u}}_i$ and $\hat{\boldsymbol{u}}_{i-1}$, $\boldsymbol{\theta}_i$ is given by (21). The points ${}^{wt}\boldsymbol{x}_i$ are projected onto a geometric estimation of the cranking task as the function (22). Equation (18)-(22) are illustrated on the right of Fig. 7.

$$\hat{\boldsymbol{u}} = (\boldsymbol{x}_o - \boldsymbol{x}_c)/(\|\boldsymbol{x}_o - \boldsymbol{x}_c\|) \tag{18}$$

$$\hat{\boldsymbol{v}} = \hat{\boldsymbol{n}} \times \hat{\boldsymbol{u}} \tag{19}$$

$$\hat{\boldsymbol{u}}_i = (\boldsymbol{x}_i - \boldsymbol{x}_c)/(\|\boldsymbol{x}_i - \boldsymbol{x}_c\|) \tag{20}$$

$$\theta_i = \operatorname{atan}(\hat{\boldsymbol{u}}_i \times \hat{\boldsymbol{u}}_{i-1}, \hat{\boldsymbol{u}}_i^T \hat{\boldsymbol{u}}_{i-1}) \tag{21}$$

$$\boldsymbol{x}_i = r\cos\theta_i\ \hat{\boldsymbol{u}} + r\sin\theta_i\ \hat{\boldsymbol{n}} \times \hat{\boldsymbol{u}} + \boldsymbol{x}_c \tag{22}$$

6) Path concatenations and deletions: The task data is no longer an amorphous set of positions and forces, but definite geometric functions that are modified, scaled, abstracted, purged, combined or transformed. For the insertion and extraction optimum trajectories, new paths are added to close gaps of deleted irregular demonstration data for example: the back and forth cranking during insertion and extraction, jerking and wiggling during chamfer crossing and extrapolation to the robot datum. Using the task space descriptions and their known orientations, task features with fixed or relative reference provide a basis of handles used for spatial transformations.

Fixed task reference define physical features and objects acquired from the DTM such as motion terminals, datums and insertion frames. Relative features, define task features that modify a task

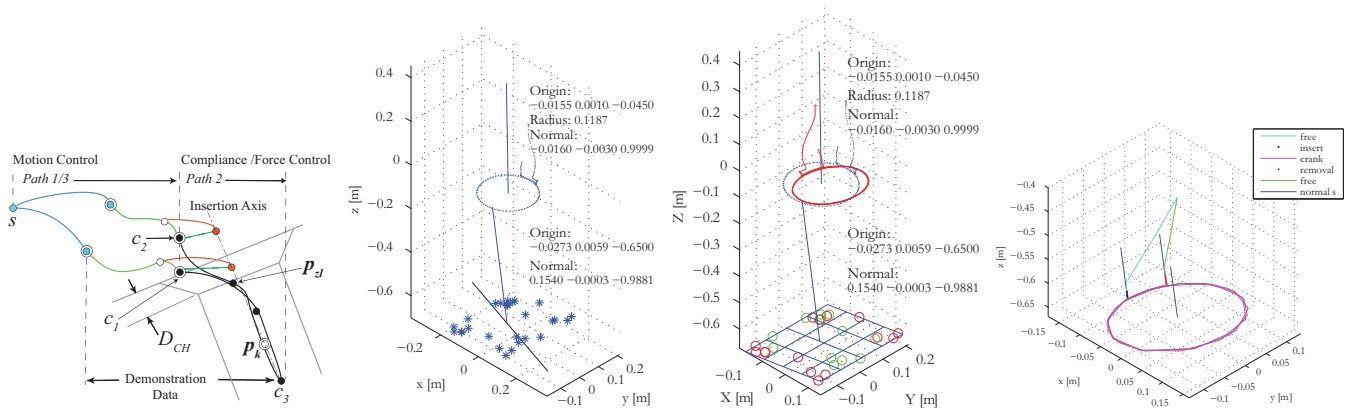

(a) Data interpretation (b) Superimposed workspaces (c) Transformations (d) Reconstructed task

Fig. 1. The constrained demonstration data interpretation is shown in (a) [2]. The demonstration workspace superimposed on the teaching workspace (b), and it shows the necessary transformation to align the two in (c) (17). The objective, to reconstruct the task in the robot reference frame, is shown in (d).

and satisfy local constraints. Trajectory segments are added to the task for stability and to achieve optimal spatial properties, with the emphasis on reconstructing the original profile of the task. On the contrary, concatenation and deletion of a task feature is done to de-emphasise the original profile and prioritise the goal objective. Intuitive human skill superimposition of dexterous motion falls under this.

A nascent motion path concatenation and deletion is based on the assumption that task reference features defined over a region of a task, remains valid in the vicinity of that region provided it describes a function of motion that satisfies $\boldsymbol{P}\ \forall\ \{\ \boldsymbol{p},\ \dot{\boldsymbol{p}},\ \ddot{\boldsymbol{p}}\ \}$ at the motion boundaries where segment points are sequentially added or removed. A task concatenation is defined by (23) and (24), for linear motion from a known feature $\boldsymbol{p}_n$, along the vector of direction $\hat{\boldsymbol{n}}$, and at $\Delta\theta$ from $\boldsymbol{p}_n$ along a curvature of radius, r, respectively. At the boundaries the task satisfies (25) and (26) for an added segment and a removed segment respectively.

$$\boldsymbol{q}_k = \mu_k \hat{\boldsymbol{n}} \tag{23}$$

$$\boldsymbol{q}_k = r\Delta\theta_k \tag{24}$$

$$\boldsymbol{p}_{n+k} = \boldsymbol{p}_n + \boldsymbol{q}_k \tag{25}$$

$$\boldsymbol{p}_{n-k} = \boldsymbol{p}_n - \boldsymbol{q}_k \tag{26}$$

Here, $k = 1, 2, ..., end$ defines a new segment that satisfies the local spatial constraints, the kinematics and continuity. Specifying the local spatial constraints ensures that non-spatial parameters such as force and stiffness of features in the vicinity are applied to the nascent feature patches, or purged.

IV. Demonstrations and Intuitive Skills

Analysis of position and force task data for: contact presence, the type of constrained contact, the motion trend under the constraint, accuracy, and estimation of regular structure in the data; consistent representation across the disparate specific objective oriented models; and simple motion combinations to create complex skill, constitute the bulk of the algorithm. This approach is used to reconstruct the inherent demonstrated motion objective from a highly irregular demonstration. Intuitive skill represented as: position, reference force and stiffness is used to improve contact. Task representation is re-cast as geometric regular functions, and intuitive motion skills are superimposed on the plain motion. Constrained and unconstrained paths in the trajectory are identified, task frame estimation, task space disambiguation, inverse kinematics data analysis, optimal path substitutions, intuitive skill integration are implemented and evaluated.

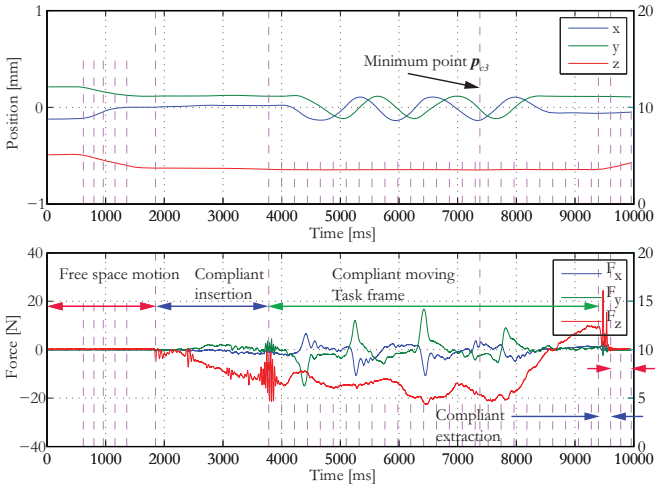

Fig. 2. Position and force data from the demonstration, three types of purple vertical lines are used: the lines 0-20 indicate the fixed features: start of contact, start of cranking, the lowest insertion point, the end of cranking and the end of extraction; the shorter lined 0-15 indicate free motion sampling nodes; the shortest lines 0-5 show the moving task frames under constrained motion.

A. Intuitive Task Reconstruction

From the human demonstration data, Fig. 2, to the reconstruction of the task result, Fig. 1(d): 1, raw data synchronisation (6); 2, motion fragmentation into constrained and unconstrained trajectories (7); 3, identification of types of constrained motion (13), (14); 4, replacement of inaccurate motion, estimation of optimum linear geometries (3),(4),(5) and (15); 5, replacing the amorphous position data with definite analytic functions (22); 6, replacement of unusable motion data and interpolation between the purged sections with analytic functions (23)-(26) are done. The resulting data in Fig. 1(d) has been fitted onto an accurately calibrated worktable (1)-(5), and is pre-experimental-evaluated for consistence Fig. 3(b).

B. Human Skill Evaluation

The reconstructed robot data in Fig. 3 was subjected to tests to evaluate the effect on the measured experimental force and exper-

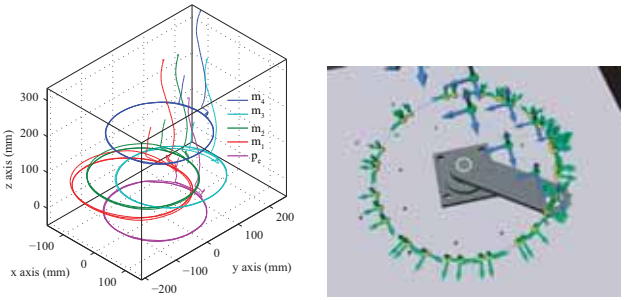

(a) Raw position data (b) Robot task data.

Fig. 3. From the markers $\boldsymbol{m}_1$ to $\boldsymbol{m}_4$ the demonstration position of the end effector $\boldsymbol{p}_e$ is computed. The intuitive algorithm reconstructs the raw position data (a) into the accurate robot task data (b).

imental errors, when the reference force, stiffness, and accuracy before insertion of the end effector are altered. The effect of force is instrumental in reducing the contact forces by setting an opposing reference force $\boldsymbol{F}_d$ in [1]. The effect of increasing the stiffness $\boldsymbol{K}$ reduced the forces since it improved trajectory following. Since accuracy was rigorously eliminated in the calibration, this observation is consistent with the theory of the method. Altering the positioning accuracy along the end effector presented interesting findings. Insertion into a rigid hole was shown earlier, however using a movable crank hole with the same parameters was not directly successful. By superimposing clockwise and counter clockwise oscillations on the insertion motion segment, a more compliant insertion motion was realised Fig. 6, and snapshots of the task are shown in Fig. 8. The two motion segments of insertion (time 1.0-2.0 [s]) and extraction (time 4.0-5.0 [s]) was reconstructed from the same geometric function of the form (23) and this must have similar force profiles without human skill. Comparing the two segments on the force and torque graphs, there is a substantial reduction in the force and torque. The intuitive human skill is inspired from the physical skill displayed by performing the task by hand. Although the clearance is sufficient to insert the peg freely, moving the robot end effector mounted peg is more prone to jamming. Jamming is eased by twisting around the insertion axis. While the robot has higher positioning accuracy, unlike humans, during insertion the rate of motion slows down due to adverse contact, slight misalignment and friction, if the static friction threshold is crossed, the slip-stick effect sets in to change the dynamics of insertion. Fig. 7 (*left*), shows the limiting friction behaviour of the robot model, the superimposed twisting motion maintains the velocity at both the constrained surface and the robot motors above the static friction threshold to achieve lower sliding friction.

C. Stiffness Estimation

Hand stiffness is determined by linearising the measured hand force and displacement [13], a least sqaures polynomial fit of the force data provides a global approximation of the force data used in the linearisation. At each perturbation the stiffness is computed by integration over the interval and the maximum stiffness is extracted. Perturbation data for computing the stiffness Fig. 4, and the stiffness model generated Fig. 5 estimate the task model stiffness.

V. Conclusions and Future Work

A. Conclusions

In order to demonstrate the robustness of intuitive human skill motion on constrained control, a comparison of skillful and plain accurate geometric task data were used for the same tasks. A faster and easier motion generation method was presented, embedding an

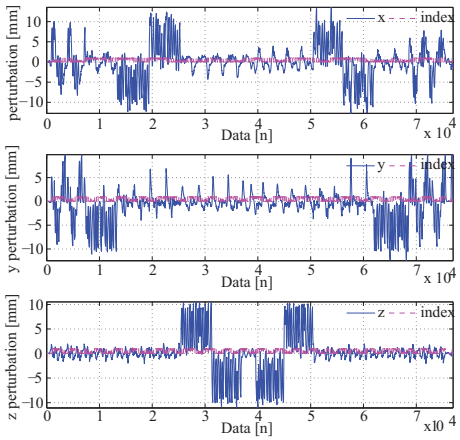

Fig. 4. 24 perturbations at 8 equally spaced points along a horizontal circular trajectory, in the directions $\pm x, \pm y, \pm z$, half in the clockwise, and half in anti-clockwise cranking direction are shown for the x, y and z axes.

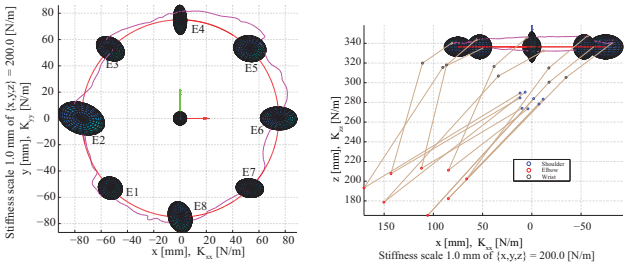

Fig. 5. Hand postures and stiffness ellipsoids are shown, they constitute the stiffness model for peg cranking.

intuitive algorithm before the GUI, its use mitigates the difficulties and time spent in building the various sections of the trajectory data when using only the simulated virtual environment. The stiffness model for the insertion task, determined experimentally (HPM), was used to avert reliance on complex mathematical models, which are difficult to create. The stiffness model was abstracted to the cranking task using an intuitive task motion generation algorithm. 1, the intuitive algorithm adds a level autonomous decision control to the teaching system and does not necessitate a precisely structured demonstration environment; 2, task motion segmentation, parameter specification and estimation and geometric optimisation of the teaching data is achieved and was verified practically; 3, the task is reconstructed into analytic geometric functions with the possibility of mathematical operations, and abstractions; 4, to isolate the effects of other factors, and limiting adverse contact forces depended on an accurately configured workspace using the DKM; 5, position errors and force measured from HPM were used in a comparative analysis of a more autonomous motion generation algorithm (HDM); 6, Contact force was used to analyse the effect of intuitive human skill reconstruction, mimicking dexterous skillful motion which showed a substantial reduction in constrained contact forces, and overcoming larger errors preceding contact.

B. Related and Future Work

Motion capture of the hand postures and applying a method [13] of analysis to determine hand stiffness has been done. Three parameters, position, force and stiffness form the major inputs to the constrained motion phase. This paper has dealt with the first and second parameters, by the replacement of the amorphous teaching position data with explicit geometric functions, functions subject to geometric mathematical methods. This is most useful

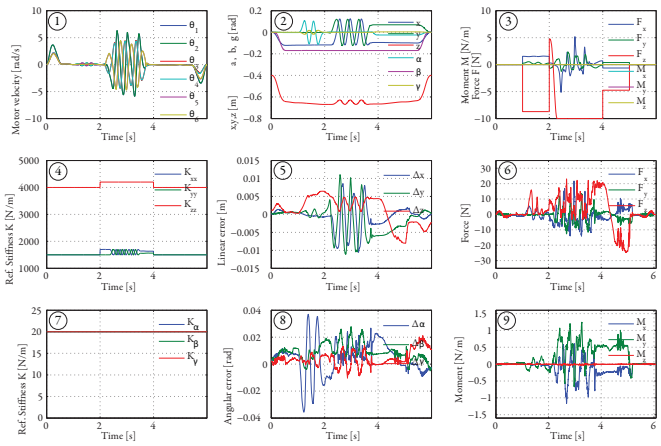

Fig. 6. In the sub-figures shown, 1. shows the reference velocity superimposition of dexterous skill between time 1-2 [s]. Originally the motion between 1-2 [s] and 4-5 [s] was linear, but the force during insertion exceeded the safe working limits, by skill superimposition the forces and torques in sub-figures (6) and (9) are substantially reduced between 1-2 [s]. The insertion was more robust to insertion errors with a 100% insertion success rate. Sub-figures (2), (3), (4) and (7) show the experiment position, force, linear and angular stiffness reference values respectively

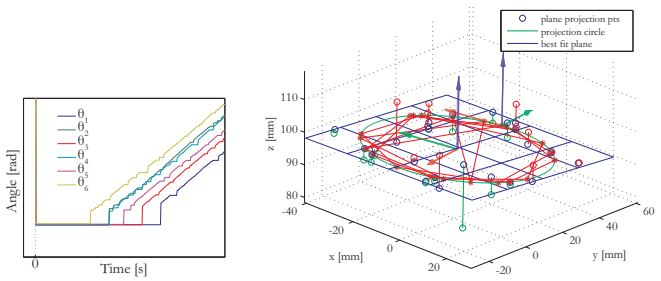

Fig. 7. Stick-slip friction behaviour at low motor velocities (*left*). A regular function (circle) estimated from an irregular trajectory (*right*). Trajectory perturbation nodes, red circle above, blue green circles below a least squares estimation projection circle (regular function)

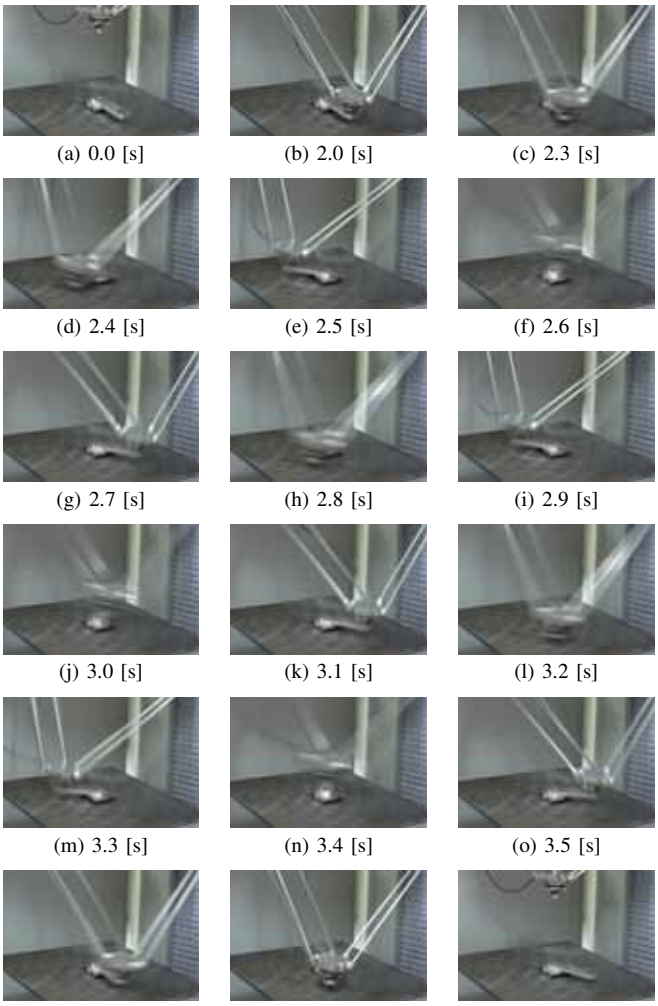

(a) 0.0 [s] (b) 2.0 [s] (c) 2.3 [s]
(d) 2.4 [s] (e) 2.5 [s] (f) 2.6 [s]
(g) 2.7 [s] (h) 2.8 [s] (i) 2.9 [s]
(j) 3.0 [s] (k) 3.1 [s] (l) 3.2 [s]
(m) 3.3 [s] (n) 3.4 [s] (o) 3.5 [s]
(p) 3.6 [s] (q) 3.7 [s] (r) 6.0 [s]

Fig. 8. Evaluation experiment showing the control of high speed motion by compliance without force feedback.

when the demonstration data significantly deviates from the *a priori* geometric function. This approach is useful when dealing with estimation of the third parameter, stiffness. In the model to estimate the stiffness, an active teaching environment is setup using a 6-DOF haptic device to give perturbations to the hand which distorts the measured geometric data, but the inherent task, as a regular function (shown to the right of Fig. 7), is recovered by the algorithm of this paper and simultaneous estimation of position, force and stiffness is achieved.

References

[1] M. Uchiyama and D. Sato, "Dexterous motion design for a directdrive parallel robot", *Robotics Research, The 11th International Symposium*, pp. 26–35, 2005.

[2] S. Okodi, X. Jiang, A. Konno, and M. Uchiyama, "Human demonstration data for fast task teaching", *Proc. of the 2008 IEEE International Conference on Intelligent Robot Systems*, pp. 961–966, 2008.

[3] D. Sato, R. Kobayashi, A. Kobayashi, and M. Uchiyama, "Task teaching system for a force-controlled parallel robot using multiple teaching modes with human demonstration data", *Proceedings of the IEEE International Conference on Robotics and Automation*, pp. 3960–3965, 2006.

[4] T. Yoshikawa, "Force control of robot manipulators", *Proceedings of the 2000 IEEE International Conference on Robotics and Automation*, pp. 220–226, 2000.

[5] I.T. Pietsch, M. Kreft, O.T. Becker, C.C. Bier, and J. Hesselbach, "How to reach the dynamic limits of parallel robots? an autonomous control approach", *IEEE Transactions on Automation Science and Engineering*, vol. 2, no. 4, pp. 369–380, October 2005.

[6] U. Thomas, F.M. Wahl, J. Maass, and J. Hesselbach, "Towards a new concept of robot programming in high speed assembly applications", *Proceedings of the 2005 IEEE International Conference on Robotics and Automation*, pp. 3932–3938, 2005.

[7] S.R. Chhatpar and M.S. Branicky, "Search strategies for peg-in-hole assembly with position uncertainty", *Proceedings of 2001 IEEE/RSJ International Conference on Intelligent Robots and Systems*, pp. 1465–1470, 2001.

[8] Yasuo Kuniyoshi, Masayuki Inaba, and Hirochika Inoue, "Learning by watching: Extracting reusable task knowledge from visual observation of human performance", *IEEE Transactions on Robotics and Automation*, vol. 10, no. 6, pp. 799–822, 1994.

[9] Katsushi Ikeuchi and Takashi Suehiro, "Toward an assembly plan from observation part i: Task recognition with polyhedral objects", *IEEE Transactions on Robotics and Automation*, vol. 10, no. 3, pp. 368–385, 1994.

[10] Sing Bing Kang and Katsushi Ikeuchi, "Toward automatic robot instruction from perception – temporal segmentation of tasks from human hand motion", *IEEE Transactions on Robotics and Automation*, vol. 11, no. 5, pp. 670–681, 1995.

[11] F. Peirrot and M. Uchiyama, "A new design of a 6-dof parallel robot", *Journal of Robotics and Mechatronics*, vol. 2, no. 4, pp. 308–315, 1990.

[12] I.M. Smith (editor), "Least squares geometric elements library", 2002.

[13] T. Flash and F. Mussa-Ivaldi, "Human arm stiffness characteristics during the maintenance of posture", *Experimental Brain Research*, vol. 82, pp. 315–326, 1990.